Electrochromic Nanocrystal Quantum Dots

Congjun Wang, *et al.*

Science **291**, 2390 (2001);
DOI: 10.1126/science.291.5512.2390

Electrochromic Nanocrystal Quantum Dots

Congjun Wang, Moonsub Shim, Philippe Guyot-Sionnest*

Incorporating nanocrystals into future electronic or optoelectronic devices will require a means of controlling charge-injection processes and an understanding of how the injected charges affect the properties of nanocrystals. We show that the optical properties of colloidal semiconductor nanocrystal quantum dots can be tuned by an electrochemical potential. The injection of electrons into the quantum-confined states of the nanocrystal leads to an electrochromic response, including a strong, size-tunable, midinfrared absorption corresponding to an intraband transition, a bleach of the visible interband exciton transitions, and a quench of the narrow band-edge photoluminescence.

Nanometer-scale materials promise to be important in the development of next-generation electronic and optoelectronic devices. Colloidal semiconductor nanocrystals are particularly attractive (*1*–*3*) because their color is directly determined by their dimension. This effect arises from the uncertainty relation that makes the energies of an electron or hole increase as the wave functions are confined to a smaller space. We show that adding electrons can lead to further control over the optical properties of these "artificial atoms" (*4*, *5*). In addition to the electrochromic properties, semiconductor nanocrystals are the subject of much interest for use in electroluminescent displays (*6*, *7*) or photovoltaic cells (*8*). In seeking to improve these devices, it will be necessary to determine the energies of electron and hole injection, or reduction and oxidation potentials. The reduction potential is now measured by combining spectroscopic and electrochemical methods.

Electrochromic materials, in which the optical properties change in response to application of an electric current (*9*, *10*), are widely studied for their use in applications such as displays and solar control windows, with current materials often based on nanocrystalline metal oxides (*11*). After injection of an electron into the nanocrystalline matrix, chromatic changes result from optical transitions induced from the newly occupied surface states and/or accumulation of electrons in the conduction band. Despite the nanometer-sized scale providing a large surface area to enhance the efficiency of electron injection, no manifestation of the quantum confinement effect has been observed in these materials, to the best of our knowledge.

II-VI and III-V semiconductor quantum dots such as CdSe, ZnSe, and InP (*12*–*14*) are known for the size-tunable atomic-like properties arising from quantum confinement in the nanometer scale. Colloidal nanocrystals of these semiconductors display striking absorption features and strong fluorescence from the ultraviolet (UV) to the infrared (IR) arising from their "artificial atom" character. Changing the "oxidation number" of the nanocrystal colloids by placing electrons into the quantum-confined states (rather than in surface states) has only recently been achieved by using electron transfer from a reducing species in solution (*15*). Furthermore, the electron injection in the quantum-confined states has been shown to lead to marked changes in the absorption and fluorescence properties (*15*, *16*). Here we show that electrons can be reversibly injected in the quantum-confined states of nanocrystals by using an electrochemical potential control. Although electrochemical reduction of ZnO nanocrystals has been reported (*17*), electrons were most likely placed in surface trap states.

Colloidal nanocrystals of CdSe and CdSe/ZnS (core/shell) are prepared by established methods (*12*, *18*). All solvents and reagents are dried by standard techniques before use. Solutions containing nanocrystals in tetrahydrofuran (THF) with 0.1 M tetrabutylammonium perchlorate (TBAP) as supporting electrolyte are loaded into a spectroelectrochemical cell (*19*) with a CaF_2 window. The Pt electrode is a 6.25-mm optically polished disk, spaced about 300 μm from the window. The potential of the Pt electrode is controlled by a potentiostat with respect to a Ag pseudo-reference electrode. The Ag pseudo-reference is calibrated with a ferrocene/ferrocenium redox couple. The Ag pseudo-reference is offset from the standard hydrogen electrode (SHE) by 0.1 V, and all potentials reported are with respect to the Ag pseudo-reference, unless otherwise noted. A Pt wire is used as the counterelectrode. By means of a Fourier transform IR spectrometer and a fiber-optic UV-visible spectrometer, the IR and the visible absorption spectra of the solution are recorded simultaneously by monitoring the reflection from the Pt electrode. Photoluminescence spectra are obtained at a 90° angle.

In the IR and visible spectra of CdSe nanocrystals under electrochemical potential (Fig. 1, A and B), a critical value can be seen around which large optical changes are observed. The new mid-IR absorption is an optical transition between the lowest quantum-confined state 1S and the next higher state manifold 1P. This IR absorption provides direct evidence that the injected electrons are placed in the 1S state. Because the 1S state is occupied, there is also a bleach of the lowest interband exciton transition. The bleach magnitude is a measure of the overall concentration of reduced nanocrystals in the probed volume because one-electron occupation of the 1S state would lead to a 50% bleach. In Fig. 1, A and B, the visible bleach is 10% and

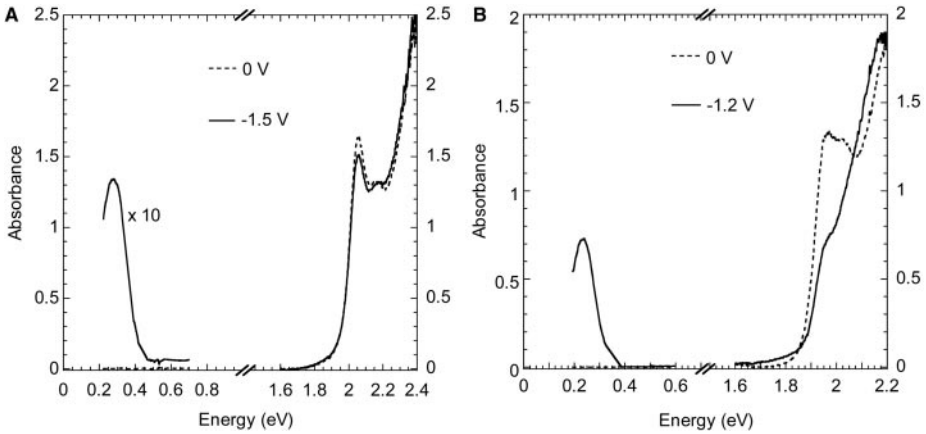

Fig. 1. IR and UV-visible spectra of (**A**) 5.4-nm CdSe nanocrystals, and (**B**) 7.0-nm CdSe nanocrystals at different potentials. Between 0.35 and 0.45 eV, the solvent C-H stretch blocks out the IR source, and hence the absorbance in this range is omitted for clarity.

James Franck Institute, University of Chicago, Chicago, IL 60637, USA.

*To whom correspondence should be addressed. E-mail: pgs@uchicago.edu

50%, corresponding to about 20% and 100%, respectively, of reduced nanocrystals within the probed volume. Two-electron injection, corresponding to 100% bleach, should in principle be observable at a potential higher than the one-electron injection by charging energy, but we have not yet observed such a step. The bleach magnitude is most likely determined by a kinetic equilibrium between oxidative processes, which are faster for smaller sizes (*16*), and the reduction originating at the electrode. Eliminating diffusion by using thin films of nanocrystals directly deposited on the electrode would improve the magnitude and the rate of electrochromic changes (*20*).

In the past, a combination of optical and infrared spectroscopy and reduction by reducing species in solution or electrochemical potential has been used to infer the reduction potential (defined as the potential at which electrons occupy the quantum-confined states) for oxide colloids and nanocrystalline films (*17*, *21*, *22*). Our approach is similar except that the intraband spectroscopy unambiguously identifies the injection of electrons in the quantum-confined state. In Fig. 2, the quasi–steady state IR absorbance of the colloids is shown as a function of the applied potential. The data are fitted to the redox equilibrium determined by the reduction potential, V_R, where the absorbance is taken to be proportional to $\exp[-e(V - V_R)/kT]/\{1 + \exp[-e(V - V_R)/kT]\}$, where e is the elementary charge, k is the Boltzmann constant, and T is the temperature. The extracted reduction potential for nanocrystals with an average diameter of 3.0, 5.4, and 7.0 nm is −1.57, −0.91, and −0.80 V, respectively (versus SHE). In the inset to Fig. 2, the confinement energy (first exciton energy minus bulk band gap of 1.7 eV) is compared with the measured reduction potential. The line is a simple approximation of the size-dependent reduction potential as the sum of the confinement energy, charging energy, and the bulk reduction potential (*23*). Extrapolating to zero confinement energy, the bulk reduction potential should be −0.3 V (versus SHE). This should be the flatband potential of bulk *n*-CdSe/trioctylphosphine oxide (TOPO) in the THF solution with TBAP as the electrolyte, which has not been measured. Comparison with reported values of flatband potentials is not fruitful at this stage because these values vary by more than 1.5 V, depending on the surface preparation and the choice of electrolyte (*24*, *25*). Indeed, the reduction potential of 7.0-nm-diameter CdSe nanocrystals capped with octanethiol is −1.07 V, whereas the reduction potential of the same-sized nanocrystals capped with TOPO is −0.80 V (versus SHE). Therefore, the measurements described above will need to be performed for each type of surface-capping group of the colloids.

One of the most notable aspects of electrochemical electron injection is the reversibility of electrochromic changes of the nanocrystal colloids. The IR absorption arising from the electron occupation of the 1S state can be turned on and off by changing the applied potential (Fig. 3). The drift in the IR absorption from cycle to cycle may be due to the drift in the pseudo-

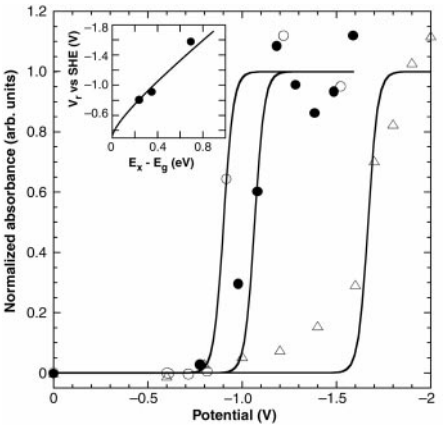

Fig. 2. The dependence of IR absorption on the applied potential. IR absorption of 3.0-nm- (△), 5.4-nm- (●), and 7.0-nm- (○) diameter CdSe nanocrystals is shown. The lines are least-square fits based on electrochemical equilibrium considerations described in the text. (**Inset**) The dependence of the reduction potential (V_R), at which electrons are injected into the 1S state of nanocrystals, on the confinement energy, $E_x - E_g$. E_x is the first exciton transition energy measured from the optical absorption spectrum. E_g is the room temperature bulk band gap.

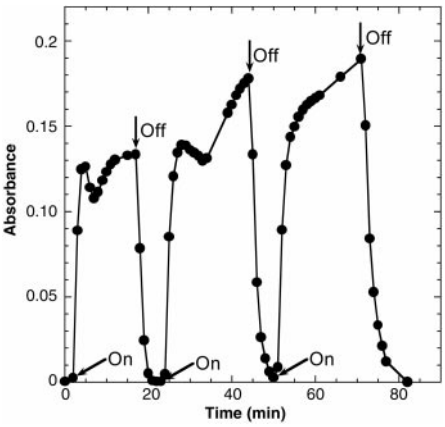

Fig. 3. IR absorption of 5.4-nm CdSe nanocrystals at different potentials. The intraband absorption at 0.27 eV is turned on by applying −1.5 V potential and turned off by resetting the potential to 0 V. The arrows labeled "On" and "Off" indicate that the potential is set to −1.5 V and reset to 0 V, respectively.

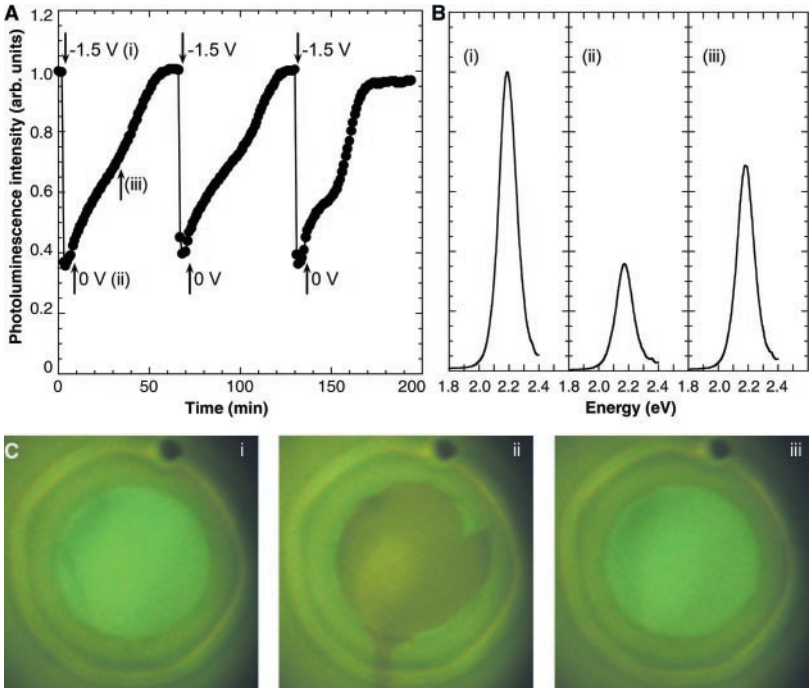

Fig. 4. (**A**) Integrated photoluminescence intensity of CdSe/ZnS core/shell nanocrystals (core diameter 4 nm) at different potentials. The photoluminescence is quenched at −1.5 V and recovers at 0 V. The photoluminescence may be quenched further at longer duration of applied potential or at higher potentials. (**B**) Photoluminescence spectra at 0 V (i), at 3 min after setting the potential to −1.5 V (ii), and at 25 min after resetting the potential to 0 V (iii). (**C**) Photographs of the sample cell illuminated by a handheld UV lamp at 0 V (i), 3 min after applying a potential of −1.5 V (ii), and 25 min after resetting the potential to 0 V (iii). The exposure time is the same in all three images.

reference potential as well as slight decomposition (as indicated by a small amount of black precipitate collecting on the electrodes after several hours). The ~2-min rise and decay times of the IR absorption are due to cell geometry and the slow mobility of the nanocrystals. Larger nanocrystals exhibit slower time constants.

Applying a potential to a solution of CdSe nanocrystals also induces quenching of the band-edge photoluminescence. Whether delocalized in a quantum-confined state or localized in a surface state, charges can cause marked quenching of the photoluminescence in semiconductor nanocrystals (*16*). The same effect is observed in the electrochemical electron injection. The "on/off" behavior of the photoluminescence properties of CdSe/ZnS core/shell nanocrystals is seen (Fig. 4A) as the electrochemical potential is varied (set at either 0 or −1.5 V). The photoluminescence spectra of CdSe/ZnS (Fig. 4B) correspond to points (i), (ii), and (iii) in Fig. 4A. The photographs of the sample under UV illumination (Fig. 4C) show that photoluminescence quenching is readily observed by eye and occurs mostly near the working-electrode disk. The spatial selectivity of photoluminescence quenching may be desirable in display applications.

At −1.5 V, the photoluminescence quenches to ~40% of the initial value in 1 min and recovers completely in ~60 min after the potential is reset to 0 V. The slower photoluminescence recovery rate with respect to the IR absorption decay may be attributed to the effects of surface charges; that is, the IR absorption depends only on the electrons in the 1S state, whereas the photoluminescence can be strongly quenched by charges in the surface band-gap states. For the photoluminescence to recover to its maximum, electrons in both the 1S state and surface states need to be removed. Improvements in surface passivation, experimenting with different electrolytes and different materials, and investigating thin solid-film electrodes are likely to lead to technologically practical and efficient electrochemical switching of the optical properties of colloidal nanocrystal quantum dots.

References and Notes

1. M. Nirmal, L. E. Brus, *Acc. Chem. Res.* **32**, 407 (1999).
2. A. P. Alivisatos, *Science* **271**, 933 (1996).
3. C. B. Murray, C. R. Kagan, M. G. Bawendi, *Science* **270**, 1335 (1995).
4. M. A. Kastner, *Phys. Today*, 24 (1993).
5. R. C. Ashoori, *Nature* **379**, 413 (1996).
6. V. Colvin, M. Schlamp, A. P. Alivisatos, *Nature* **370**, 354 (1994).
7. B. O. Dabbousi, M. G. Bawendi, O. Onitsuka, M. F. Rubner, *Appl. Phys. Lett.* **66**, 1316 (1995).
8. B. O'Regan, M. Grätzel, *Nature* **353**, 737 (1991).
9. T. Yamase, *Chem. Rev.* **98**, 307 (1998).
10. C. G. Granqvist, *Sol. Energ. Mat. Sol. Cells* **60**, 201 (2000).
11. U. zum Felde, M. Haase, H. Weller, *J. Phys. Chem. B* **104**, 9388 (2000).
12. C. B. Murray, D. J. Norris, M. G. Bawendi, *J. Am. Chem. Soc.* **115**, 8706 (1993).
13. M. A. Hines, P. Guyot-Sionnest, *J. Phys. Chem. B* **102**, 3655 (1998).
14. O. I. Micic *et al.*, *J. Phys. Chem.* **98**, 4966 (1994).
15. M. Shim, P. Guyot-Sionnest, *Nature* **407**, 981 (2000).
16. M. Shim, C. Wang, P. Guyot-Sionnest, *J. Phys. Chem. B*, in press.
17. P. Hoyer, H. Weller, *Chem. Phys. Lett.* **221**, 379 (1994).
18. M. A. Hines, P. Guyot-Sionnest, *J. Phys. Chem.* **100**, 468 (1996).
19. R. E. Wittrig, C. P. Kubiak, *J. Electroanal. Chem.* **393**, 75 (1995).
20. We have not yet observed hole injection most likely because of other oxidative processes that prevent it. Applying a positive potential (0 to +3 V) to the samples did not cause changes in the visible absorption or photoluminescence properties of the nanocrystals. Successful hole injection will require an optimization of solvent and electrolyte combination as well as nanocrystals that are stable after oxidation.
21. N. M. Dimitrijevic, D. Savic, O. I. Micic, A. J. Nozik, *J. Chem. Phys.* **88**, 4278 (1984).
22. B. Enright, G. Redmond, D. Fitzmaurice, *J. Phys. Chem.* **98**, 6195 (1994).
23. The confinement energy, $E_x - E_g$, can be approximated as $\hbar^2/2m^*R^2$ and the charging energy, E_c, as $e^2/2\varepsilon R$. E_x is the first exciton transition energy, E_g is the bulk band gap, R is the radius of the nanocrystals, m^* is the effective mass of the electron, and ε is the dielectric constant of the solvent. With the bulk reduction potential, V_0, the reduction potential, V_R, of nanocrystals can be expressed as $[(E_x - E_g) + E_c]/e + V_0$.
24. R. Memming, *Top. Curr. Chem.* **169**, 105 (1994).
25. R. J. D. Miller, G. L. McLendon, A. J. Nozik, W. Schmickler, F. Willig, *Surface Electron Transfer Processes* (VCH, New York, 1995), p. 44.

26. Funded by a grant from the National Science Foundation (DMR-9731642). Experiments made use of the Materials Research Science and Engineering Centers Shared Facilities supported by a grant from the National Science Foundation (DMR-9400379).

28 November 2000; accepted 1 February 2001

In Situ Measurement of Grain Rotation During Deformation of Polycrystals

L. Margulies,[1,2] G. Winther,[1] H. F. Poulsen[1]*

Texture evolution governs many of the physical, chemical, and mechanical properties of polycrystalline materials, but texture models have only been tested on the macroscopic level, which makes it hard to distinguish between approaches that are conceptually very different. Here, we present a universal method for providing data on the underlying structural dynamics at the grain and subgrain level. The method is based on diffraction with focused hard x-rays. First results relate to the tensile deformation of pure aluminum. Experimental grain rotations are inconsistent with the classical Taylor and Sachs models.

Most metals and ceramics are aggregates of crystalline grains. The crystalline lattice of each grain has a characteristic orientation, and a polycrystal is thus characterized by a distribution of orientations—its texture. The texture plays a role in virtually every modern industry, determining phenomena as disperse as the weight of beer cans and the prospect of high-temperature superconducting cables. The orientation difference between neighboring grains is the focus of an emerging technology termed "grain boundary engineering." At the same time, textures in minerals and rocks are vital sources revealing information about geological processes.

Textures evolve during plastic deformation, where a polycrystal changes its shape. At the grain level, each grain changes its shape and its crystallographic lattice rotates. The external force produces line defects (dislocations) in the lattice. The dislocations move in certain directions (slip directions) within certain planes (slip planes), causing the two sides of the plane to slide with respect to each other. The change in grain shape is the result of millions of such operations. The dynamics of the grains are coupled, because the two sides of any grain boundary at all times must adjoin and be in stress equilibrium. To facilitate this process, the grains have to change shapes in different ways, and their crystallographic orientations must rotate with respect to each other.

Various texture models have been presented in the literature for more than 50 years. They predict which possible slip systems (combinations of slip plane and slip direction) are operational and calculate the resulting texture and other macroscopic properties,

[1]Materials Research Department, Risø National Laboratory, 4000 Roskilde, Denmark. [2]European Synchrotron Radiation Facility, BP 220, 38043 Grenoble, France.

*To whom correspondence should be addressed. E-mail: henning.friis.poulsen@risoe.dk